CONF-881207--3

FRACTURE TOUGHNESS OF $MgCr_2O_4$-BASED REFRACTORY COMPOSITES*

J. P. Singh and R. B. Poeppel

Materials and Components Technology Division
Argonne National Laboratory
Argonne, Illinois 60439 USA

CONF-881207--3

DE89 009847

November 1988

INVITED TALK to be presented at the Seventh SIMCER (7th International Symposium on Ceramics), Bologna, Italy, December 14-16, 1988.

*Work was supported by the U. S. Department of Energy, Office of Fossil Energy, Advanced Research and Technology Development Materials Program, under Contract W-109-Eng-38.

FRACTURE TOUGHNESS OF $MgCr_2O_4$-BASED REFRACTORY COMPOSITES

J. P. Singh and R. B. Poeppel
Materials and Components Technology Division
Argonne National Laboratory
Argonne, Illinois 60439 USA

ABSTRACT

The effects of unstabilized ZrO_2 and W inclusions on the fracture surface energy and thermal-shock resistance of $MgCr_2O_4$ have been characterized. The fracture surface energy increased with increasing ZrO_2 content to a maximum value of 24.5 J/m^2 at 16.5 vol. % ZrO_2, and decreased as the ZrO_2 content increased further. The increase in fracture surface energy for $MgCr_2O_4$-W with increasing W content was monotonic for the range of composition studied ($\leq$10.3 vol.% W); a value of 26 J/m^2 was obtained for $MgCr_2O_4$-10.3% W composites. It is proposed that these fourfold increases in fracture surface energy result from the absorption of energy due to microcrack formation in the $MgCr_2O_4$ matrix, which results from the tensile stresses due to the mismatch in thermal expansion coefficient and/or elastic modulus between the matrix and inclusions. In addition, for $MgCr_2O_4$-ZrO_2 composites, a major cause of microcracking is the tetragonal → monoclinic phase transformation of ZrO_2 and the associated volume expansion. Thermal quench experiments indicated substantial improvements in the thermal-shock resistance of $MgCr_2O_4$ with appropriate ZrO_2 and W additions.

I. INTRODUCTION

Refractory linings for the main pressure vessel of slagging coal gasifiers are subjected to very corrosive environments (molten slag) and to thermal shock caused by the temperature fluctuations [1]. These conditions may result in refractory degradation by corrosion, cracking and spalling [2-4]. As indicated by Kennedy [5], refractory degradation by corrosion and thermal shock has been reported in several pilot plants, including the converted Lurgi-type gasifier [6,7] operated by the British Gas Council and the Bi-Gas pilot plant [8]. In view of the good resistance to corrosion by molten slag, high-chromia refractories (specifically with a $MgCr_2O_4$ spinel phase) appear to be very promising candidates for slagging coal gasifier applications [9-12]. Unfortunately, these high-chromia refractories have relatively poor resistance to thermal-shock fracture [13]. For long service life, these refractories should have good thermal-shock as well as corrosion resistance.

The thermal-shock resistance of refractories is often predicted by the well-known thermal-shock-resistance parameters R'''' and R_{st} [14,15]. These parameters have been derived by Hasselman for a brittle material with uniformly distributed penny-shaped cracks with no crack interactions [16]. An increase in R'''' corresponds to a decrease in the final crack length resulting from the propagation of an initially small crack due to thermal shock. On the other hand, R_{st} is proportional to the minimum temperature difference required to initiate the propagation of large cracks under thermal-shock conditions. These parameters increase with increasing fracture surface energy γ, and a high value of γ will result in improved thermal-shock resistance.

The fracture surface energy, γ, of brittle materials can be improved by incorporating second-phase inclusions. These inclusions may act as crack-arresting sites [17-19] or induce microcracking [20-22] in the matrix which may absorb energy and thus increase the fracture surface energy. Microcracking in the matrix results from the tensile stresses caused by the mismatch between the thermal expansion coefficients, and/or the elastic moduli, of the matrix and the inclusions. An example of the application of expansion coefficient mismatch to cause microcracking and hence improve thermal-shock resistance is the addition of W inclusions in a MgO matrix [23]. The tensile stresses may also include large matrix stresses around inclusions due to the volume change of the inclusions during phase transformation. Microcracking as a result of phase transformation in unstabilized ZrO_2 has been successfully utilized to improve the fracture toughness of Al_2O_3 [20,21]. Unstabilized ZrO_2 goes through a tetragonal → monoclinic phase change at ~1030°C with an associated linear expansion of ~1.4% [24]. This expansion induces high stresses and associated microcracking at the interface of the ZrO_2 inclusions and the particular matrix, e.g., Al_2O_3, when the material is cooled from the fabrication (sintering, hot pressing) temperature, and results in an increase in fracture surface energy. The purpose of the present study was to study the effect of unstabilized ZrO_2 and W inclusions on the fracture surface energy of $MgCr_2O_4$-ZrO_2 and $MgCr_2O_4$-W composites.

II. MATRIX STRESSES AND CRITICAL INCLUSION SIZE

For microcracking to occur in the $MgCr_2O_4$ matrix around inclusions, the tensile stress in the matrix should exceed the fracture stress for $MgCr_2O_4$ and the particle size of the inclusions should be equal to or greater than a critical value R_c [25]. Following Claussen [20], the tensile stress was estimated by using Selsing's [26] equation for stresses around a spherical particle in an isotropic matrix:

$$\sigma_r = -2\sigma_t = \frac{-(\alpha_m - \alpha_p)\,\Delta T}{\frac{1+\nu_m}{2E_m} + \frac{1-2\nu_p}{E_p}} (R/r)^3, \qquad (1)$$

where m and p refer to matrix and inclusion, respectively, σ_r is the radial stress, σ_t is the tangential stress, r is the radial distance from the inclusion, R is the radius of the inclusion, α is the expansion coefficient, ν is Poisson's ratio, E is the elastic modulus, and ΔT is the difference between room temperature and the maximum temperature below which the stresses are no longer relaxed during cooling. To account for the effect of expansion as a result of tetragonal → monoclinic phase transformation, the linear expansion of 1.4% was added in the numerator. The value of ΔT was assumed to be 1000°C. From Eq. (1), it can be seen that the maximum σ_t occurs at the interface (r = R). From the properties values shown in Table I, the maximum values of σ_t were calculated to be 1229 MN/m^2 for ZrO_2 and 345 MN/m^2 for W inclusions, which are much larger than the fracture stress of the $MgCr_2O_4$ matrix (~66 MN/m^2); this result suggests the possibility of microcrack formation in the matrix if ZrO_2 and W particles are of the critical size. The critical particle size of ZrO_2 and W inclusions (R_c) for microcrack formation was estimated from the equation proposed by Davidge and Green [24]:

$$R_c \geq 8\gamma_s / \left(P^2\{(1+\nu_m)/E_m + 2\,(1-2\nu_p)/E_p\}\right), \qquad (2)$$

where

$$P = \frac{(\alpha_m - \alpha_p)\,\Delta T}{\frac{1+\nu_m}{2E_m} + \frac{1-2\nu_p}{E_p}},$$

and γ is the value of fracture surface energy evaluated for the material without inclusions. The other symbols have been defined earlier. Substituting the properties values of Table I in Eq. (2), one obtains R_c = 0.6 μm for ZrO_2 and 9.5 μm for W inclusions. Preliminary observations of the polished surfaces of $MgCr_2O_4$-ZrO_2 and $MgCr_2O_4$-W composites indicated that a major portion of the agglomerate ZrO_2 particles were larger than 0.6 μm and ~20% of W particles were 9.5 μm or larger. These preliminary estimations suggest that the composites satisfy the conditions of critical stress and

TABLE I. Mean Properties of ZrO_2-W and $MgCr_2O_4$

Property	$MgCr_2O_4$[a]	Monoclinic ZrO_2[b]	W[c]
Expansion coefficient, α (10^{-6} $^oC^{-1}$)	8.1	7.15[b]	4.5
Elastic modulus, E (GN/m^2)	159	200	345
Poisson's ratio, ν	0.26	0.29	0.283
Surface energy, γ (J/m^2)	5.9	-	-

[a]Present work.
[b]Value of expansion coefficient taken from Ref. 27; other values assumed.
[c]Ref. 28.

inclusion particle size that are required for the occurrence of microcracking in the $MgCr_2O_4$ matrix around the ZrO_2 and W inclusions.

III. EXPERIMENTAL PROCEDURES

$MgCr_2O_4$ powder was made by wet ball milling the appropriate amounts of dried $MgCO_3$* and Cr_2O_3* for 16 h in methanol with Al_2O_3 balls. The slurry mixture was dried in room temperature air and then calcined at 1200°C for 4 h in air. The structure of the calcined mixture was identified as $MgCr_2O_4$ by x-ray diffraction. $MgCr_2O_4$-ZrO_2 and $MgCr_2O_4$-W composites were made by mixing $MgCr_2O_4$ powder with appropriate amounts of ZrO_2 and W and then wet ball milling the mixtures for 16 h in methanol with Al_2O_3 balls. The wet mixtures were dried in room temperature air. The dried mixtures were mixed with 5% acryloid-stearic acid (4:1) binder system dissolved in methanol. Methanol was evaporated from the mixtures by slow heating. The dry mixtures were ground and sieved through a 30-mesh screen. Rectangular bar specimens (~5.1 x 0.6 x 0.3 and 5.1 x 0.6 x 0.6 cm) of the composites were pressed in a steel die at ~103 MN/m^2. These bars were sintered at 1650°C for 1-1/3 h at oxygen partial pressures ranging from $\sim 9 \times 10^{-13}$ to 10^{-11} atm.

*Laboratory grade, Fisher Scientific Co., Fair Lawn, NJ.

After sintering, the density measurements and microstructural evaluation of each set of composite specimens were completed to ensure the reproducibility of high density and uniform fine-grain microstructure. Subsequently, mechanical and thermal-shock properties were evaluated.

The smaller bars (~5.1 x 0.6 x 0.3 cm) were used to measure strength in four-point bending with a support span of 3.8 cm, a loading span of 2.2 cm and a cross-head speed of 0.13 cm/min. The larger bars (~5.1 x 0.6 x 0.6 cm) were used to measure fracture toughness (critical stress intensity factor, K_{IC}) by the notch beam technique [29] (NBT) with a notch width of ~0.04 cm. The elastic modulus (E) was measured by the pulse-echo technique [30]. The fracture surface energy (γ) was calculated from the relation $\gamma = K_{IC}^2/2E$ for plane stress conditions. Slightly different values of γ will be obtained from the plane strain relation $\gamma = K_{IC}^2 (1 - \nu^2)/2E$. The difference between the two cases will be small for the typical values of Poisson's ratio $\nu \simeq 0.2$-0.3. It is also to be noted that plastic deformation in $MgCr_2O_4$ has been assumed to be very limited and γ represents an effective fracture surface energy which includes energy forms other than thermodynamic surface energy.

The thermal-shock resistance of $MgCr_2O_4$ and its composites was measured by quenching rectangular bar specimens (~5.1 x 0.6 x 0.3 cm) at various temperatures into room temperature silicone oil* with a nominal viscosity of 5×10^{-6} m^2s^{-1} at 25°C. The specimens were slowly heated to predetermined temperatures in an electrically heated furnace, held at that temperature for ~15 min to attain thermal equilibrium, and dropped into the silicone oil bath. Four specimens were used for each test condition. Mechanical degradation of the specimens was determined by measuring their flexural strength before and after the thermal quench.

IV. RESULTS AND DISCUSSIONS

A. Microstructure

The sintered specimens of $MgCr_2O_4$, $MgCr_2O_4$-ZrO_2 and $MgCr_2O_4$-W composites had densities $\geq$94, 96.4, and 93.9% of theoretical value,† respectively. $MgCr_2O_4$ and its composites had a fine-grain (grain

*Type 200, Dow Corning Corp., Midland, MI.

†Theoretical densities were calculated by using the rule of mixture. The values for the theoretical densities of $MgCr_2O_4$, W, and ZrO_2 were taken to be 4.42, 19.3, and 5.6 g/cm^3, respectively.

size <15 μm) and relatively uniform microstructure. Figures 1-3 show typical scanning electron micrographs of the fracture surfaces of the specimens of $MgCr_2O_4$ and its composites; a mixed intergranular and transgranular mode of fracture is evident. The particle size distribution of the second phase (ZrO_2 or W) was obtained by measuring the agglomerate particle sizes of ZrO_2 and W on the polished surfaces of as-sintered specimens of the $MgCr_2O_4$-ZrO_2 and $MgCr_2O_4$-W composites. The agglomerate particle size of ZrO_2 in $MgCr_2O_4$-ZrO_2 composites ranged from 0.4 to 7 μm, with ~1.5 μm the most frequent particle size [31]. The agglomerate particle size distribution of W particles for $MgCr_2O_4$-W composites ranged from ~1 to 33 μm, with 6 μm the most frequent particle size [32]. These distributions suggest that most of the ZrO_2 particles and ~20% of the W particles were larger than their respective critical particle sizes R_c (0.6 μm for ZrO_2, 9.5 μm for W) for the formation of microcracks.

B. Mechanical Properties

Table II summarizes the measured values of flexural strength (σ_f), elastic modulus (E), fracture toughness (K_{IC}) and fracture surface energy (γ) as a function of ZrO_2 content for $MgCr_2O_4$-ZrO_2 composites. A plot of the elastic modulus data (Fig. 4) shows that the elastic modulus for $MgCr_2O_4$-ZrO_2 composites decreases with increasing ZrO_2 content for ZrO_2 contents greater than 7.3%. The decrease in elastic modulus values indirectly suggests the existence of microcracking in the $MgCr_2O_4$ matrix due to ZrO_2 inclusions. The initial increase in the elastic modulus value is probably due to the higher elastic modulus of ZrO_2 (~200 GN/m^2) as compared with pure $MgCr_2O_4$ (~160 GN/m^2) and the very limited microcracking.

Figure 5 shows the dependence of flexural strength (σ_f) and fracture surface energy (γ) (from Table II) on the volume fraction of ZrO_2. These results indicate that there is little change in γ for ZrO_2 contents $\leq$7.3%, probably because there is little or no microcracking in the matrix for these compositions. At higher ZrO_2 contents, interaction between the stress fields of adjacent ZrO_2 particles may have resulted in a critical stress condition at the matrix-inclusion interface and consequent microcracking of the matrix. The density of microcracks ahead of the notch tip during fracture toughness (K_{IC}) measurements increased with increasing ZrO_2 content; this increase probably resulted in more energy absorption [20,21] with a corresponding increase in γ. At 16.5% ZrO_2 content, γ reached a maximum value of 24.5 J/m^2. This represents an approximately fourfold increase in the fracture surface energy of $MgCr_2O_4$ with ZrO_2 inclusions as compared with the value of $MgCr_2O_4$ without any inclusions. Similar improvements have been observed for Al_2O_3 with ZrO_2 inclusions [20,21]. With a further increase in ZrO_2 content, microcracks start joining up to form macrocracks; this process

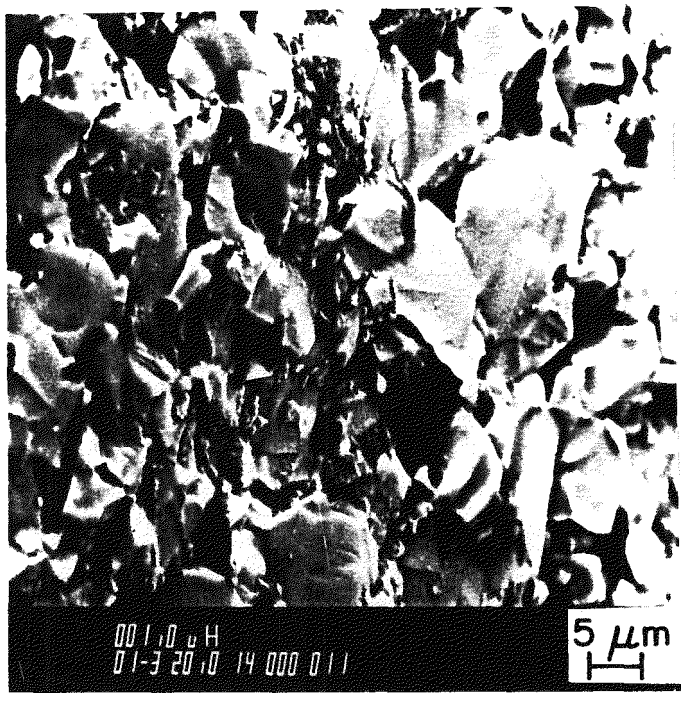

Fig. 1. Typical scanning electron micrograph of fracture surface of $MgCr_2O_4$.

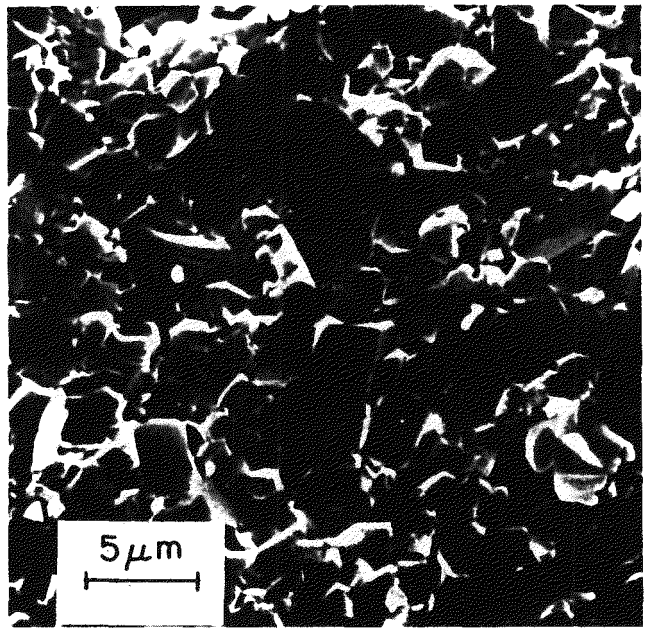

Fig. 2. Typical scanning electron micrograph of fracture surface of $MgCr_2O_4$ + 7% ZrO_2 composite.

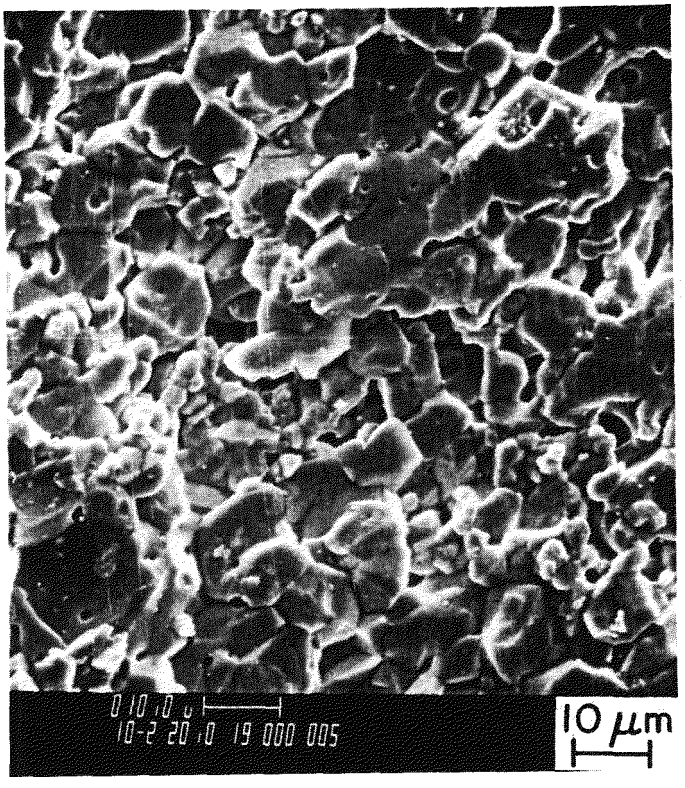

Fig. 3. Typical scanning electron micrograph of fracture surface of $MgCr_2O_4$ + 5% W composite.

TABLE II. Measured Properties of $MgCr_2O_4$-ZrO_2 Composite Specimens with Different Volume Fractions of ZrO_2 Inclusions

ZrO_2 (vol. %)	Flexural Strength, σ_f (MN/m^2)	Elastic Modulus, E (GN/m^2)	Critical Stress Int. Factor, K_{IC} ($MN/m^{3/2}$)	Fracture Surface Energy,[a] γ_{NBT} (J/m^2)
0	66 ± 7	158 ± 2	1.36 ± 0.05	5.9 ± 0.4
3.8	120 ± 15	175 ± 2	1.49 ± 0.06	6.4 ± 0.5
7.3	105 ± 15	186 ± 3	1.54 ± 0.02	6.3 ± 0.1
10.6	132 ± 11	-	1.79 ± 0.06	8.9 ± 0.6
13.6	137 ± 31	174 ± 0	2.26 ± 0.17	14.8 ± 2.2
16.5	154 ± 25	166 ± 3	2.84 ± 0.18	24.2 ± 3.0
21.6	132 ± 31	166 ± 1	2.42 ± 0.13	17.7 ± 1.9

[a] γ_{NBT} was calculated from the measured value of K_{IC}.

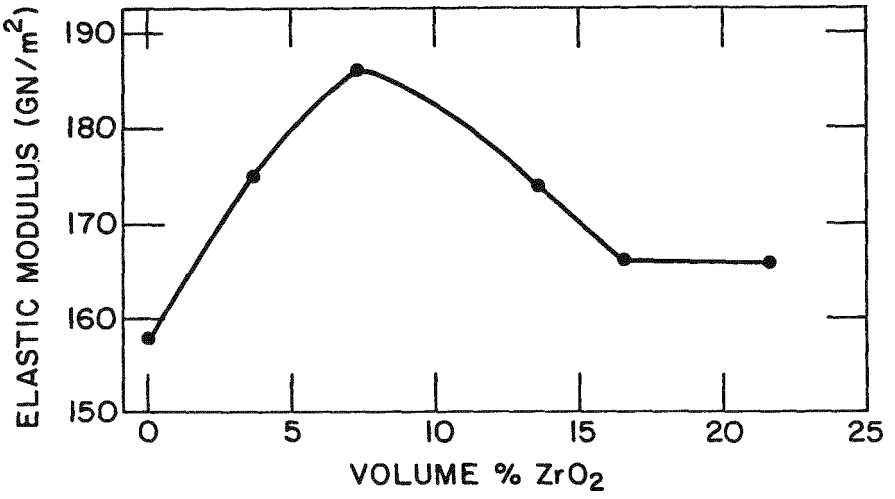

Fig. 4. Dependence of elastic modulus on ZrO_2 content in $MgCr_2O_4$-ZrO_2 composites.

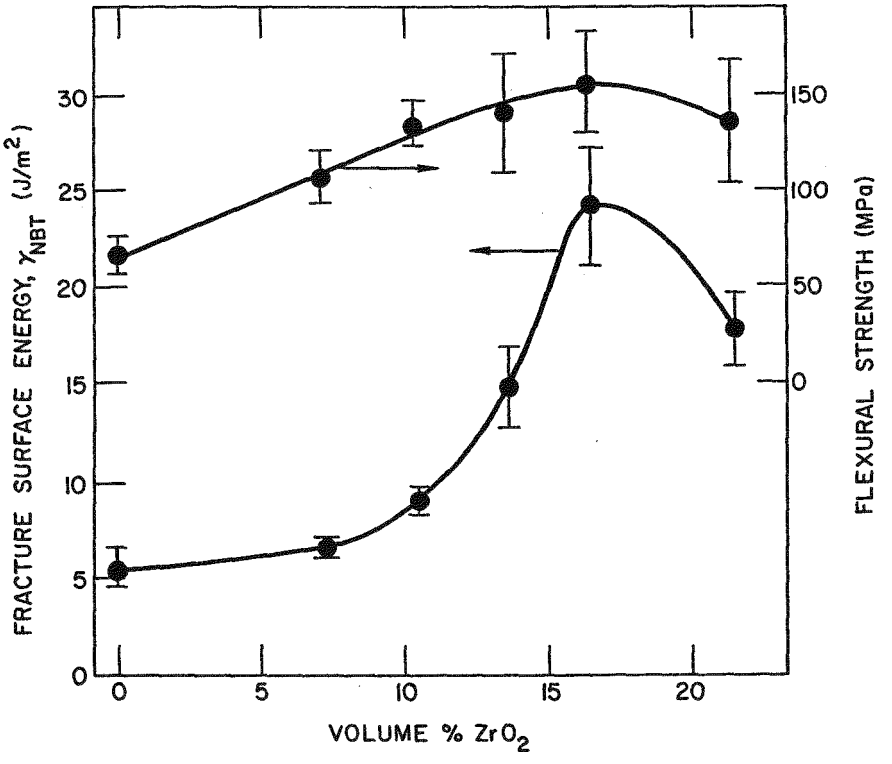

Fig. 5. Dependence of strength and fracture surface energy on ZrO_2 content in $MgCr_2O_4$-ZrO_2 composites.

facilitates crack propagation and thus decreases the fracture surface energy. The strength plot in Fig. 5 shows similar trends, i.e., the strength increases with increasing ZrO_2 content, reaches a maximum value of 154 MN/m^2 at 16.5% ZrO_2 content, and starts to decrease for ZrO_2 contents greater than 16.5% because of macrocrack formation.

The measured values of mechanical properties of $MgCr_2O_4$-W composites are summarized in Table III. Data from Table III have been plotted in Fig. 6 to show the dependence of the elastic modulus of $MgCr_2O_4$-W composites on W content. It is seen in Fig. 6 that the elastic modulus increases with increasing W content for W $\leq$5.4%. This increase presumably results from a combination of the limited amount of microcracking and the higher elastic modulus of W (~345 GN/m^2) as compared with $MgCr_2O_4$. As in the case of $MgCr_2O_4$-ZrO_2 composites (Fig. 4), the elastic modulus of $MgCr_2O_4$-W composites decreases with further increases in W content (>5.4% W); this behavior suggests the formation of microcracks. This observation directly relates to the fracture surface energy results of Table III, which are plotted in Fig. 7. As shown in Fig. 7, there is only a small increase in the fracture surface energy of $MgCr_2O_4$-W composites for W content $\leq$5.4%, consistent with little or no microcracking for these compositions. On the other hand, for W contents >5.4%, microcrack density increases, as suggested by the elastic-modulus results. The increase in microcrack density results in more absorption of elastic energy and a corresponding increase in γ. The strength of $MgCr_2O_4$-W composites increases with increasing W content, reaches a maximum value at 7.4% W content, and starts to decrease for higher W contents. Unlike $MgCr_2O_4$-ZrO_2 composites (Fig. 5), $MgCr_2O_4$-W

TABLE III. Measured Properties of $MgCr_2O_4$-ZrO_2 Composite Specimens with Different Volume Fractions of W Inclusions

W (vol. %)	Flexural Strength, σ_f (MN/m^2)	Elastic Modulus, E (GN/m^2)	Critical Stress Int. Factor, K_{IC} ($MN/m^{3/2}$)	Fracture Surface Energy,[a] γ_{NBT} (J/m^2)
0	66 ± 7	158 ± 2	1.36 ± 0.05	5.9 ± 0.4
1.1	63 ± 3	156 ± 3	1.74 ± 0.19	9.8 ± 2.2
3.3	90 ± 15.7	185 ± 12	1.97 ± 0.11	10.4 ± 1.1
5.4	124 ± 6.7	201 ± 2	2.18 ± 0.12	11.9 ± 1.4
7.4	133 ± 12.3	188 ± 17	2.44 ± 0.17	15.9 ± 2.2
10.3	111 ± 11.2	129 ± 3	2.58 ± 0.13	26.0 ± 2.5

[a] γ_{NBT} was calculated from the measured value of K_{IC}.

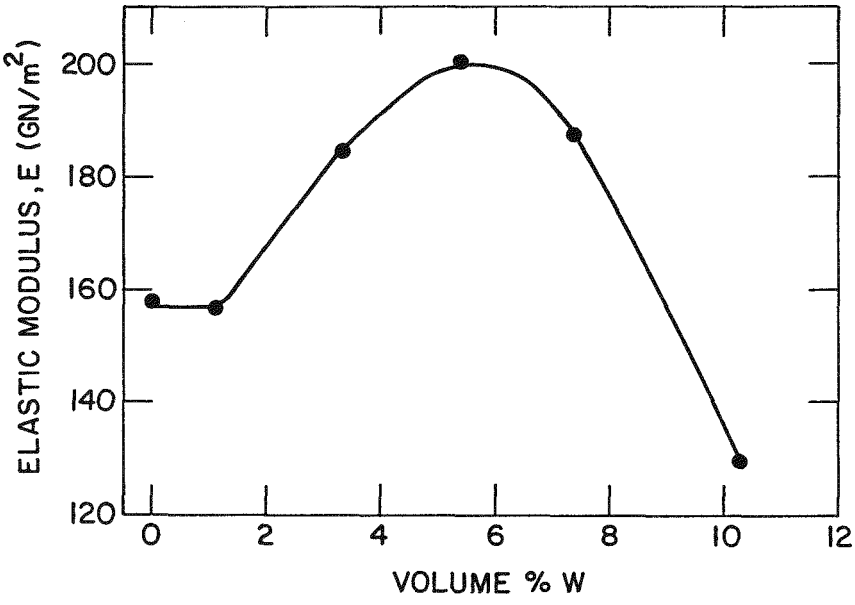

Fig. 6. Dependence of elastic modulus on W content in $MgCr_2O_4$-W composites.

composites started to decrease in strength (for >7.4% W) while the fracture surface energy was still increasing. This observation is probably due to a nonuniform distribution of W particles as compared with ZrO_2 particles. Nonuniformly distributed W particles could induce a few large isolated cracks which would cause strength degradation without decreasing the fracture surface energy.

It is important to note that at 16.5% ZrO_2, the $MgCr_2O_4$-ZrO_2 composites have both high γ and high strength. Strength and γ were also found to increase with W content for W $\leq$7.4%. Similar observations were reported by Becher [21] for Al_2O_3-ZrO_2 composites, but in another study, strength was found to decrease as a result of microcracking. The increase in both γ and strength in the present work is proposed to be due to the small size and uniform distribution of the microcracks, which result from the small size and uniform distribution of the ZrO_2 and W inclusions. As Claussen [20] has also proposed, energy absorption by uniformly distributed small microcracks can increase γ while a small critical crack size is maintained so that the strength is not adversely affected.

In view of the fact that fracture surface energy data for candidate commercial refractories for slagging gasifier application are generally available as work of fracture (γ_{WOF}), a direct comparison will require γ_{WOF} measurements for the $MgCr_2O_4$ base refractory

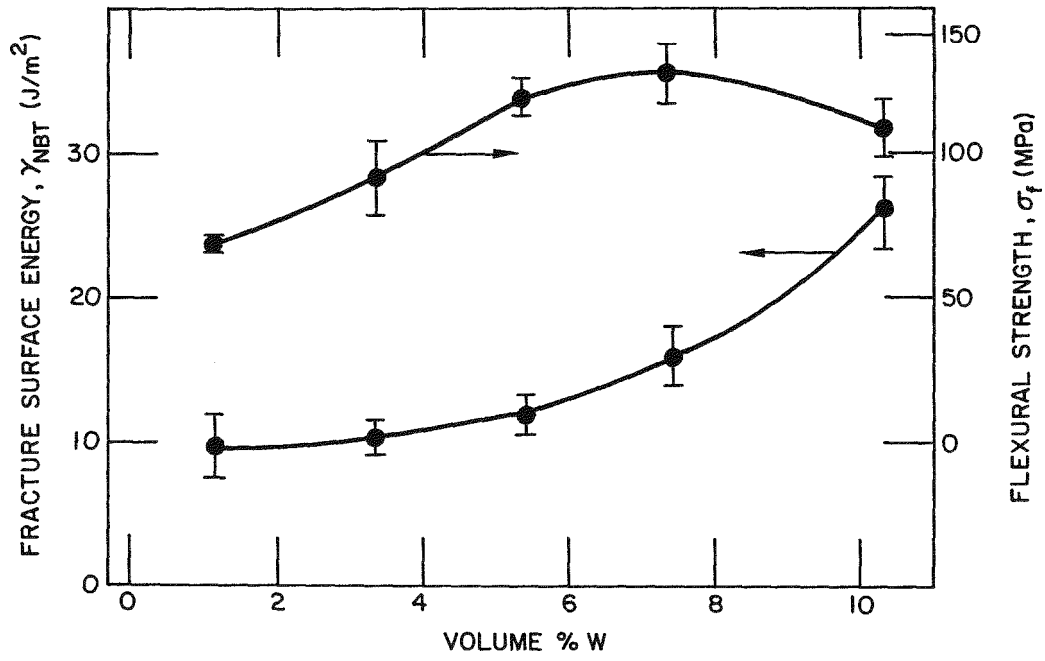

Fig. 7. Dependence of strength and fracture surface energy on W content in $MgCr_2O_4$-W composites.

composites. For γ_{WOF} measurement, a stable mode of fracture is required. This was very difficult to achieve with small-size composite specimens. Further attempts with larger specimens, along with other modifications in the measurement techniques, have been deferred to a later date.

C. Thermal-Shock Behavior

In view of the fourfold increase in the value of γ for $MgCr_2O_4$ with ZrO_2 and W inclusions, $MgCr_2O_4$-ZrO_2 and $MgCr_2O_4$-W composites were tested to evaluate the improvements in their thermal-shock resistance.

The results of the thermal-shock experiments are presented in Fig. 8, which shows the retained strength of specimens subjected to varying degrees of thermal quench (ΔT). The results indicate a substantial improvement in the thermal-shock resistance of $MgCr_2O_4$-ZrO_2 composites as compared with pure $MgCr_2O_4$. The value of the critical quenching temperature difference (ΔT_c) for strength degradation due to thermal shock is ~350°C for $MgCr_2O_4$-16.5% ZrO_2 and ~450°C for $MgCr_2O_4$-21.6% ZrO_2, as compared to ~200°C for pure $MgCr_2O_4$. The retained strength after thermal shock for the composite specimens is also higher than that for pure $MgCr_2O_4$.

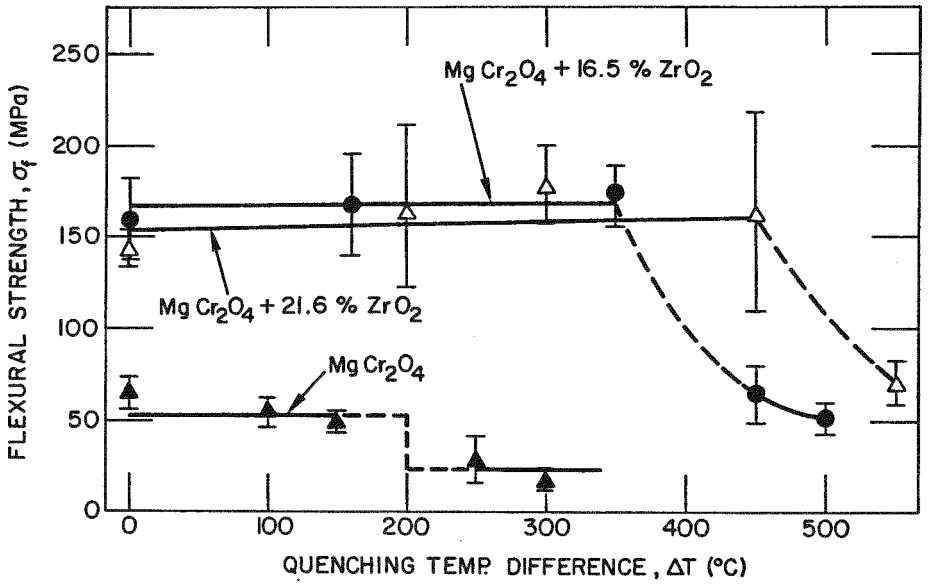

Fig. 8. Effect of ZrO_2 content on thermal-shock behavior of $MgCr_2O_4$.

Figure 9 shows the thermal-shock behavior of $MgCr_2O_4$ and its composites with 10.3% W inclusions. The composite with 10.3% W was selected for thermal-shock study because it showed substantially improved fracture surface energy. As in the case of $MgCr_2O_4$-ZrO_2 composites, substantial improvements in thermal-shock behavior were observed for $MgCr_2O_4$-W composites. The value of ΔT_c is ~400°C as compared to the value of ~200°C for pure $MgCr_2O_4$. The retained strength after thermal shock is also seen to have increased.

Although a direct comparison could not be made between γ_{WOF} values for $MgCr_2O_4$ base refractory composites and commercial refractories, the results of the thermal-shock experiments are very promising and suggest that these refractory composites will compare favorably with the commercial refractories.

V. SUMMARY

The results presented in this report for $MgCr_2O_4$ and its composites with ZrO_2 and W inclusions clearly indicate that these inclusions substantially improve mechanical and thermal-shock properties of $MgCr_2O_4$. These improvements are due to the absorption of energy due to microcrack formation in the $MgCr_2O_4$ matrix, which results from the tensile stresses due to the mismatch in thermal expansion coefficient and/or elastic modulus between the matrix and inclusions. In addition, for $MgCr_2O_4$-ZrO_2 composites, a major cause of microcracking is

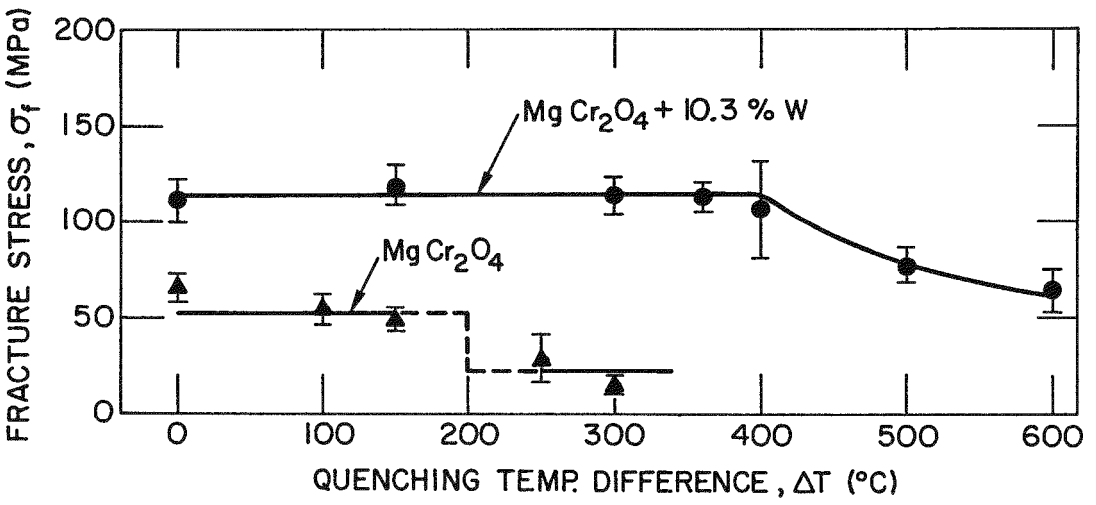

Fig. 9. Effect of W content on thermal-shock behavior of $MgCr_2O_4$.

the tetragonal → monoclinic phase transformation of ZrO_2 and the associated volume expansion. The highlights of the results are as follows:

The degree of improvement in strength and fracture surface energy of $MgCr_2O_4$ with ZrO_2 and W inclusions was found to depend on the volume fraction of ZrO_2 and W.

The flexural strength of $MgCr_2O_4$ increased from 66 MN/m^2 to 154 MN/m^2 with 16.5 vol. % ZrO_2 inclusions and to 133 MN/m^2 with 7.4 vol. % W inclusions.

The fracture surface energy of $MgCr_2O_4$ increased from 5.9 J/m^2 to 24.2 J/m^2 with 16.5 vol. % ZrO_2 inclusions and to 26 J/m^2 with 10.3 vol. % W inclusions.

The improvement in mechanical properties (specifically, the fracture surface energy) of $MgCr_2O_4$ due to ZrO_2 and W inclusions resulted in improved thermal-shock resistance of the composites. The critical quenching temperature differences for strength degradation due to thermal shock were 450°C and 400°C for $MgCr_2O_4$-21.6% ZrO_2 and $MgCr_2O_4$-10.3% W composites, respectively, as compared with 200°C for $MgCr_2O_4$. The retained strength after critical thermal shock for these composites also increased.

ACKNOWLEDGMENTS

The work was supported by the U. S. Department of Energy, Advanced Research and Technology Development Fossil Energy Materials Program, under Contract W-31-109-Eng-38. The authors thank W. A. Ellingson for his technical support throughout this work. Thanks are extended to J. J. James and J. J. Picciolo for their valuable experimental assistance.

REFERENCES

[1]. W. T. Bakker, "Refractory Applications in Coal Gasifiers," in Proc. Third Ann. Conf. on Materials for Coal Conversion and Utilization, Gaithersburg, MD, CONF-781018, pp. K103-153 (1978).

[2]. W. D. Kingery, J. Am. Ceram. Soc. 38(1) (1955) 3-15.

[3]. B. Brenzy, Am. Ceram. Soc. Bull. 58(7) (1979) 679-682.

[4]. J. Nakayama, "Thermal Shock Resistance of Ceramic Materials," in Fracture Mechanics of Ceramics, Vol. 2, pp. 759-778, eds. R. C. Bradt, D. P. H. Hasselman, and F. F. Lange, Plenum Press, New York (1974).

[5]. C. R. Kennedy, in Proc. Fourth Annual Conference on Materials for Coal Conversion and Utilization, Gaithersburg, MD, October 1979, CONF-791014, pp. K60-K94 (1979).

[6]. D. Hebden, J. A. Lacey, and A. G. Horsler, J. Inst. Gas Eng. 5 (1965) 367-382.

[7]. Refractories for Coal Gasification and Combustion Systems, EPRI Technical Report AP-1268 (July 1980).

[8]. Gas Generator Research and Development: Bi-Gas Process, Phillips Petroleum Company Quarterly Progress Report, January-March 1978, FE1207-45, p. 127 (April 1978).

[9]. C. R. Kennedy and R. B. Poeppel, Interceram 27(3) (1978) 221-226.

[10]. J. A. Bonar, C. R. Kennedy, and R. B. Swaroop, Am. Ceram. Soc. Bull. 59(4) (1980) 473-478.

[11]. C. R. Kennedy, J. Mater. Energy Syst. 2(2) (1980) 11-20.

[12]. C. R. Kennedy, "Refractory/Coal-Slag Compatibility Studies: Progress to Date," presented at Am. Ceram. Soc. Ann. Mtg., Washington, D.C. (1981).

[13]. J. P. Singh, D. R. Diercks, R. B. Poeppel, and G. Bandyopadhyay, Thermal-Shock Studies on Refractories for Slagging Coal Gasifiers, ANL/FE-84-3 (1984).

[14]. D. P. H. Hasselman, J. Am. Ceram. Soc. 52(11) (1969) 600-604.

[15]. D. P. H. Hasselman, in Materials Science Research Vol. V, Ceramics in Severe Environments, pp. 89-103, eds. W. W. Kriegel and H. Palmour, III, Plenum Press, New York (1971).

[16]. J. P. Singh, C. Shih, and D. P. H. Hasselman, Comm. Am. Ceram. Soc. 64(8) (1981) 106-109.

[17]. D. P. H. Hasselman and R. M. Fulrath, J. Am. Ceram. Soc. 49 (2) (1966) 68-72.

[18]. F. F. Lange, Philos. Mag. 22[Ser. 8] (1970) 983-992.

[19]. Dipak R. Biswas and Richard M. Fulrath, J. Am. Ceram. Soc. 58(11-12) (1975) 526-527.

[20]. N. Claussen, J. Am. Ceram. Soc. 59(1-2) (1976) 49-51.

[21]. P.F. Becher, J. Am. Ceram. Soc. 64(1) (1981) 37-39.

[22]. N. Claussen and J. Jahn, J. Am. Ceram. Soc. 61(1-2) (1978) 94-95.

[23]. R. C. Rossi, Am. Ceram. Bull. 48(7) (1969) 736-737.

[24]. R. N. Patil and E. C. Subbarao, J. Appl. Crystallogr. 2(Pt. 6) (1969) 281-288.

[25]. R. W. Davidge and T. J. Green, J. Mater. Sci. 3 (1968) 629-634.

[26]. J. Selsing, J. Am. Ceram. Soc. 44(8) (1961) 419.

[27]. R. Ruh, G. W. Hollenberg, S. R. Skaggs, S. D. Stoddard, F. G. Gas, and E. G. Charles, Am. Ceram. Soc. Bull. 60(4) (1981) 504-506.

[28]. Metals Handbook, Ninth Edition, Vol. 2, American Society for Metals (1979).

[29]. W. F. Brown, Jr., and J. E. Srawley, Amer. Soc. Test. Mater. Spec. Tech. Publ. No. 410, pp. 13-15 (1966).

[30]. J. Krautkrämer and H. Krautkrämer, Ultrasonic Testing of Materials, Springer-Verlag, New York (1983).

[31]. J. P. Singh, J. Mater. Sci., 22 (1987) 2685-2690.

[32]. J. P. Singh, R. B. Poeppel, J. J. James, and J. J. Picciolo, Development of Refractory Composites with Improved Fracture Toughness, ANL/FE-85-1 (1985).